The Locally Orthogonal Coordinate Systems for Analyzing Inverse Problems of Magnetostatic Fields

— Applications to Magnetocardiogram and Magnetoencephalogram —

Hideo Saotome and Yoshifuru Saito
College of Engineering, Hosei University
3-7-2 Kajino, Koganei, Tokyo 184, Japan

Abstract—Previously, we have proposed the sampled pattern matching (SPM) method to analyze the inverse problems in magnetostatic fields. Because of current dipole angle subdivisions, our SPM method essentially requires a considerable CPU time. In order to remove the current dipole angle subdivisions, we propose here a novel formulation of the SPM method employing the cylindrical and spherical coordinate systems. Applications of this faster SPM method to the magnetocardiogram (MCG) and magnetoencephalogram (MEG) identify the heart defect and brain activated parts, respectively.

I. INTRODUCTION

With the development of the high sensitive superconducting quantum interference device (SQUID) [1], MCG and MEG analyses have been vigorously carried out [2-6]. There is no doubt that the MCG and MEG include extremely important information for medical diagnosis. Nevertheless, diagnosis utilizing MCGs and MEGs is not yet established. In order to elicit the diagnostic information in the MCGs and MEGs effectively, it is, in essence, required to solve the inverse problems which give magnetic field sources, i.e. current distribution, from the locally measured magnetic fields.

We have previously proposed the sampled pattern matching (SPM) method in order to analyze the inverse problem and applied it to biomagnetics, such as magneto-oculogram (MOG), MCG and MEG analyses [7-11]. Moreover, the proposed algorithm has been successively applied to non-destructive testing [12]. The most outstanding merit of the SPM method is that it is possible to provide plural source positions whereas the least squares and the conventional correlative analysis give the most dominant single source [10]. Some conventional linear algebraic approaches to the inverse problem have been carried out and give plural current dipoles [13,14]. While their approaches are based on a distance between two vectors which express measured and computed magnetic fields, the SPM method evaluates an angle of the vectors.

In the previous our studies, the Cartesian coordinate system was used to estimate current dipole (or element) vectors from a measured magnetic field pattern. Identifying the spatial angle of a current dipole vector requires a considerable CPU time in the Cartesian coordinate system [9-12]. In this paper, the locally orthogonal coordinate systems, such as cylindrical and spherical coordinate systems shown in Figs. 1 and 2, are proposed for MCG and MEG analyses, respectively. Employing the proposed coordinate systems can remove the repetitive process which was inevitably necessary for the current dipole angle determination in the Cartesian coordinate system. As a result, it provides a faster SPM algorithm, which has implications for the optimal SQUID sensor configurations.

II. SYSTEM EQUATIONS FOR MCG AND MEG ANALYSES

The governing equation for MCG and MEG analyses can be expressed by the relation between the measured magnetic field intensity $\mathbf{H}$ and its source, i.e. the current density $\mathbf{J}$. The measurement of the magnetic field is not carried out in the source region, i.e. the heart and brain, but on a limited surface outside the body. Therefore, the governing equation is expressed by the following volume integral:

$$\mathbf{H} = \nabla \times \int_V G\, \mathbf{J}\, dv, \tag{1}$$

where G is the Green's function expressed by the distance between $\mathbf{J}$ and $\mathbf{H}$. The volume V contains all of the current density $\mathbf{J}$. The product $\mathbf{J}\,dv$ in (1) corresponds to the current dipole vector $\boldsymbol{\alpha}$ shown in Figs. 1 and 2.

Except for a few cases, most of presently available MCGs and MEGs are respectively composed of only the magnetic field components H_z and H_r normal to the measurement surfaces as shown in Figs. 1 and 2. Because of these measurement conditions and the rotational relation in (1), only the r and θ components of the current dipole vector $\boldsymbol{\alpha}$ can be estimated in the heart. Similarly, only the θ and ϕ components of $\boldsymbol{\alpha}$ can be estimated in MEG analysis.

Employing a cylindrical coordinate system for the MCG analysis, the magnetic field intensity H_z can be divided into two components H_{zr} and $H_{z\theta}$:

$$H_z = H_{zr} + H_{z\theta}, \tag{2}$$

where H_{zr} and $H_{z\theta}$ are caused by the r and θ components of a current dipole vector, α_r and α_θ, respectively. With e_r, e_θ and e_z denoting unit space vectors of the cylindrical coordinates, each of the magnetic fields H_{zr} and $H_{z\theta}$ in (2) are expressed by

$$H_{zr} = \frac{(\alpha_r\, e_r)\times \mathbf{s}}{4\pi |\mathbf{s}|^3} \cdot e_z, \tag{3a}$$

$$H_{z\theta} = \frac{(\alpha_\theta\, e_\theta)\times \mathbf{s}}{4\pi |\mathbf{s}|^3} \cdot e_z, \tag{3b}$$

where the distance vector $\mathbf{s}$ between H_z and $\boldsymbol{\alpha}$ is depicted in Fig. 1. In the cylindrical coordinate system, the following orthogonal relationship holds:

$$\int_P H_{zr}\, H_{z\theta}\, dS = 0, \tag{4}$$

where P refers to a circular measurement surface area shown in Fig. 1. This is because the magnetic field patterns of H_{zr} and $H_{z\theta}$ are respectively odd and even symmetrical functions with respect to the r axis shown in Fig. 1. In the commonly used Cartesian coordinate system, a similar orthogonality cannot be established:

$$\int_P H_{zx}\, H_{zy}\, dS \neq 0, \tag{5}$$

where H_{zx} and H_{zy} are the z components of the magnetic field intensities caused by the x and y components of a current dipole vector, respectively.

In the spherical coordinate system, the following formulation can be carried out similar to the cylindrical coordinate system. The magnetic field intensity H_r normal to the measure-

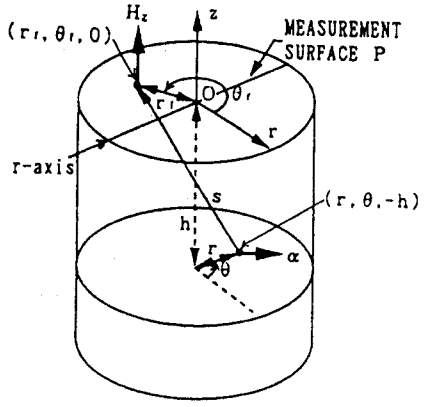

Fig. 1. The cylindrical coordinate system for the MCG analysis. $\boldsymbol{\alpha}$ denotes a current dipole vector.

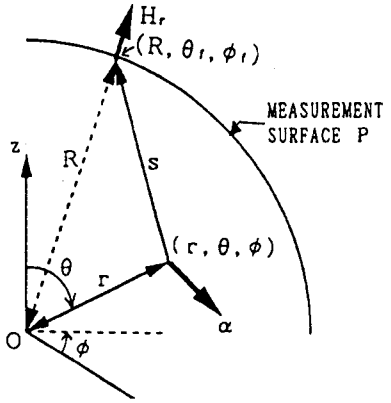

Fig. 2. The spherical coordinate system for the MEG analysis. $\boldsymbol{\alpha}$ denotes a current dipole vector.

ment surface P shown in Fig. 2 is decomposed into two orthogonal components $H_{r\theta}$ and $H_{r\phi}$:

$$H_r = H_{r\theta} + H_{r\phi}, \tag{6}$$

and

$$\int_p H_{r\theta} H_{r\phi} \, dS = 0, \tag{7}$$

is established, where $H_{r\theta}$ and $H_{r\phi}$ are caused by the θ and ϕ components of a current dipole vector, i.e. α_θ and α_ϕ, respectively. With e_r, e_θ and e_ϕ denoting unit space vectors of the spherical coordinates, $H_{r\theta}$ and $H_{r\phi}$ are given by

$$H_{r\theta} = \frac{(\alpha_\theta \, e_\theta) \times s}{4\pi |s|^3} \cdot e_r, \tag{8a}$$

$$H_{r\phi} = \frac{(\alpha_\phi \, e_\phi) \times s}{4\pi |s|^3} \cdot e_r, \tag{8b}$$

where the distance vector s is depicted in Fig. 2.

The system equations for the MCG and MEG analyses are derived from (1) with these locally orthogonal coordinate systems. By discretizing a target volume V into m subdivisions, we have

$$u = \sum_{j=1}^{m} (\alpha_{pj} \, d_{pj} + \alpha_{qj} \, d_{qj}). \tag{9a}$$

In 9(a), the vector u is a measured MCG or MEG pattern; the subscripts p and q are p=r, q=θ for the cylindrical coordinate system and p=θ, q=ϕ for the spherical coordinate system, respectively; α_{pj} and α_{qj} are the p and q components of a current dipole vector at the point j; and the vectors d_{pj} and d_{qj} are the magnetic field patterns caused by α_{pj} and α_{qj}, respectively. When we have n measurement points, u, d_{pj} and d_{qj} become the n dimensional column vectors written as

$$u = [H_{w1}, \; H_{w2}, \; \cdots, \; H_{wn}]^T, \tag{9b}$$

$$d_{pj} = \{1/(4\pi)\}[(e_{pj} \times s_{1j}) \cdot e_{w1}/|s_{1j}|^3, \; (e_{pj} \times s_{2j}) \cdot e_{w2}/|s_{2j}|^3, \; \cdots, \; (e_{pj} \times s_{nj}) \cdot e_{wn}/|s_{nj}|^3]^T, \tag{9c}$$

$$d_{qj} = \{1/(4\pi)\}[(e_{qj} \times s_{1j}) \cdot e_{w1}/|s_{1j}|^3, \; (e_{qj} \times s_{2j}) \cdot e_{w2}/|s_{2j}|^3, \; \cdots, \; (e_{qj} \times s_{nj}) \cdot e_{wn}/|s_{nj}|^3]^T. \tag{9d}$$

In (9b), (9c) and (9d), the subscript w refers to the z and r coordinates for the MCG and MEG analyses, respectively.

III. THE SPM METHOD BASED ON SPACE DOMAIN SPECTRUM THEORY

In (9a), the unknowns are α_{pj} and α_{qj}. d_{pj} and d_{qj} are determined by the geometrical relationship between the measurement and source points, as described in (9c) and (9d). u is obtained by the measurement. However, it is difficult to obtain unique solutions of α_{pj} and α_{qj} (j=1, 2, $\cdots$, m), since the following condition generally holds for MCGs and MEGs:

$$n < m, \tag{10}$$

which means the number of equations (equal to the number of the measurement points), n, is less than the number of the unknowns, m. In order to surmount this difficulty, we have developed the SPM method to obtain a solution pattern composed of current dipole spectrums in the target space domain [9, 11].

Regarding d_{pj} and d_{qj} in (9a) as basis vectors, α_{pj} and α_{qj} can be interpreted as the current dipole spectrums corresponding to the basis vectors. In order to clarify this theoretical approach, let us consider the well-known Fourier series of which the bases are the sinusoidal functions:

$$f(t) = a_0/2 + \sum_{i=1}^{\infty} \{a_i \cos(i\omega t) + b_i \sin(i\omega t)\}, \tag{11a}$$

where

$$a_0 = (2/T) \int_T f(t) \, dt, \tag{11b}$$

$$a_i = (2/T) \int_T f(t) \cos(i\omega t) \, dt, \tag{11c}$$

$$b_i = (2/T) \int_T f(t) \sin(i\omega t) \, dt, \tag{11d}$$

$$\omega = 2\pi/T. \tag{11e}$$

Comparing (9a) with (11a), it is obvious that α_{pj} and α_{qj} in the space (source) domain correspond to the spectrums a_i and b_i in the frequency domain. In the Fourier series, the basis functions $\cos(i\omega t)$ and $\sin(i\omega t)$ are orthogonal each other:

$$\int_{T/i} \cos(i\omega t) \sin(i\omega t) \, dt = 0, \tag{12}$$

even if i varies as 1, 1.1, 1.2, $\cdots$, ∞.

The most notable point of our formulations is the orthogonality:

$$d_{pj}^T \cdot d_{qj} = 0; \; p=r, \; q=\theta \text{ or } p=\theta, \; q=\phi; \tag{13}$$

due to (4) or (7) corresponding to (12). Therefore, the normalized current dipole spectrums γ_{pj} and γ_{qj} can be independently obtained by

$$\gamma_{pj} = u^T \cdot d_{pj} \; / \; (\|u\| \, \|d_{pj}\|), \tag{14a}$$

$$\gamma_{qj} = u^T \cdot d_{qj} \; / \; (\|u\| \, \|d_{qj}\|), \tag{14b}$$

since the inner products of (14a) and (14b) in the discretized system correspond to the integrations of (11c) and (11d) in the analytical system. The magnitude of a normalized current dipole spectrum, γ_j, and its spatial angle ϕ_j on the p-q plane are given by

$$\gamma_j = \sqrt{\gamma_{pj}^2 + \gamma_{qj}^2}, \tag{14c}$$

$$\phi_j = \tan^{-1}(\gamma_{qj} \; / \; \gamma_{pj}), \tag{14d}$$

where ϕ_j is determined by taking account of the signs of γ_{pj} and γ_{qj}. In the Cartesian coordinate system, normalized current dipole spectrum components are not independently evaluated because of (5). As a result, discretizing ϕ_j into subdivisions is required to determine the optimum current dipole angle.

After the process of (14a)-(14d) for j=1, 2, $\cdots$, m is completed, the following procedures are subsequently carried out in the SPM method [7-12]:

$$\gamma_{pkj} = u^T \cdot (d_{pk} + d_{pj}) \; / \; (\|u\| \, \|d_{pk} + d_{pj}\|), \tag{15a}$$

$$\gamma_{qkj} = u^T \cdot (d_{qk} + d_{qj}) \; / \; (\|u\| \, \|d_{qk} + d_{qj}\|), \tag{15b}$$

where j=1, 2, $\cdots$, m and γ_k was the maximum value among γ_1, γ_2, $\cdots$, γ_m in (14c). The evaluation of (15a) and (15b) is based on the assumption that the measured field pattern u has two N-S magnetic pole pairs due to the current dipoles located at the points k and j ($\neq$k). Then, we find out the maximum value of

$$\gamma_{kj} = \sqrt{\gamma_{pkj}^2 + \gamma_{qkj}^2}, \tag{15c}$$

for j=1, 2, $\cdots$, m. Based on the assumption of multiple N-S magnetic pole pairs, we continue the process similar to (14) and (15) up to the peak value of $\gamma_{k\cdots j}$. Finally, we get

$$\gamma_1' = \sqrt{(\gamma_{p1} + \gamma_{pk1} + \cdots)^2 + (\gamma_{q1} + \gamma_{qk1} + \cdots)^2}, \tag{16a}$$

$$\gamma_2' = \sqrt{(\gamma_{p2} + \gamma_{pk2} + \cdots)^2 + (\gamma_{q2} + \gamma_{qk2} + \cdots)^2}, \tag{16b}$$

$$\cdots\cdots\cdots\cdots\cdots\cdots\cdots\cdots\cdots\cdots,$$

$$\gamma_k' = \sqrt{(\gamma_{pk} + \gamma_{pkk} + \cdots)^2 + (\gamma_{qk} + \gamma_{qkk} + \cdots)^2}, \tag{16c}$$

$$\cdots\cdots\cdots\cdots\cdots\cdots\cdots\cdots\cdots\cdots,$$

$$\gamma_m' = \sqrt{(\gamma_{pm} + \gamma_{pkm} + \cdots)^2 + (\gamma_{qm} + \gamma_{qkm} + \cdots)^2}. \tag{16d}$$

When h is the number of repeated procedures similar to (14) and (15), we can conclude that the measured field u is composed of h pairs of N-S magnetic poles.

Each amplitude of α_{pj} and α_{qj} (j=1, 2, $\cdots$, m) in (9a) cannot be determined uniquely because of (10). However, the normalized current dipole spectrum pattern is uniquely obtained from (16). Since the basis vectors d_{pj} and d_{qj} at different points are not generally orthogonal each other, the computed spectrum pattern has some spreading bands corresponding to the frequency bands obtained by the Fourier transformation where the basis functions are not orthogonal, but the basis frequency varies continuously.

IV. CURRENT DIPOLE SPECTRUM DISTRIBUTION IN THE HEART AND BRAIN

It is well-known that the P wave in an electrocardiogram (ECG) is mainly caused by right atrial excitation. Nakaya *et al.* measured MCGs of a normal subject and a patient with right atrial overloading (RAO) during the P wave [4]. Figs. 3(a) and 4(a) are the MCGs at 33 ms and 55 ms of the normal subject. Fig. 5(a) shows the MCG at 40 ms for the RAO patient. The circles ● and ○ indicate N and S regions, respectively. Applying the proposed SPM method with the cylindrical coordinate system to these MCGs provides the current dipole spectrum patterns shown in Figs. 3(b), 4(b) and 5(b). These are visualized top 10% results obtained from (16), where m=10250 and n=21 in (9a). In these figures, the needles of the obtained current dipole spectrums indicate their positive directions; the boldface solid line denotes the heart as well as the aorta and vena cava; also the dotted line shows the ribs. As previously mentioned, the obtained spectrum patterns have spreading bands because of (10). In the normal subject, the current dipole spectrums are distributed in two regions: strongly in the vicinity of the sinoatrial node and weakly in the vicinity of the atrioventricular node. From 33 ms to 55 ms in the P wave, the obtained current dipole spectrum patterns shown in Figs. 3(b) and 4(b) have no significant difference, which coincides with the medical opinion of [4]. However, the current dipole spectrum pattern of the RAO at 40 ms, shown in Fig. 5(b), is quite different from the normal ones. In this case, the current dipole spectrums located in the right ventricular region are observed in addition to the current dipole spectrums at the sinoatrial node. Moreover, the direction of the current dipole vectors at the sinoatrial node faces the lower part compared with those of the normal ones. The strongest spectrums of Figs. 3(b) and 5(b) are located at depths of 69 mm and 30 mm from the measurement surface, respectively.

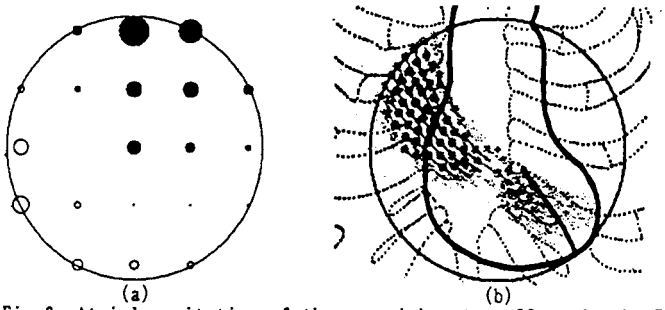

(a) (b)

Fig. 3. Atrial excitation of the normal heart at 33 ms in the P wave. (a) MCG. (b) Current dipole spectrum distribution.

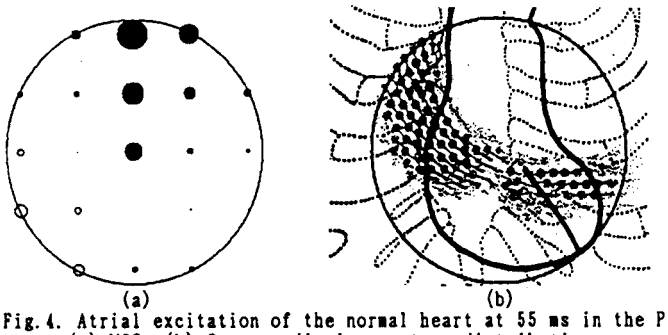

(a) (b)

Fig. 4. Atrial excitation of the normal heart at 55 ms in the P wave. (a) MCG. (b) Current dipole spectrum distribution.

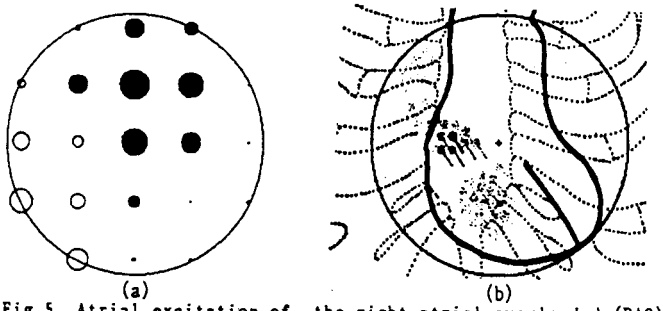

(a) (b)

Fig. 5. Atrial excitation of the right atrial overloaded (RAO) heart with the pulmonary hypertension at 40 ms in the P wave. (a) MCG. (b) Estimated current dipole spectrum distribution.

Using a 37-channel SQUID of which the sensors are mounted on a spherical surface, Kuriki *et al.* measured MEGs normal to the measurement surface, shown in Figs. 6(a) and 7(a), at 110 ms and 160 ms after a person heard the sound "ha" [6]. From the MEGs, the proposed SPM method with the spherical coordinate system produces the current dipole spectrum patterns in the brain. Figs. 6(b) and 7(b) show the top 10% results obtained from (16), where m=9843 and n=37 in (9a). The following neural activities can be observed from Figs. 6(b) and 7(b): 1) The region from the primary auditory cortex to the Wernicke's area is activated at 110 ms. 2) The angular gyrus is mainly activated at 160 ms. The results in Figs. 6(b) and 7(b) show that the activated regions play important roles for auditory functions. The strongest spectrums of Figs. 6(b) and 7(b) are located at depths of 87 mm and 52 mm from the measurement surface, respectively.

Required CPU times for the computation of the heart and brain are respectively 40 seconds and 330 seconds with HP730 EWS.

V. CONCLUSION

We have proposed the faster SPM method utilizing the locally orthogonal coordinate systems, i.e. the cylindrical and spherical coordinate systems, and applied it to MCGs as well as MEGs. The demonstrations, presented in this paper, of obtaining the current dipole spectrums in the heart and brain have succeeded in clarifying the activated and defect parts in the body. Thus, our faster SPM method suggests that SQUID sensors should be mounted on a circular or spherical surface, rather than in a square or rectangular grid.

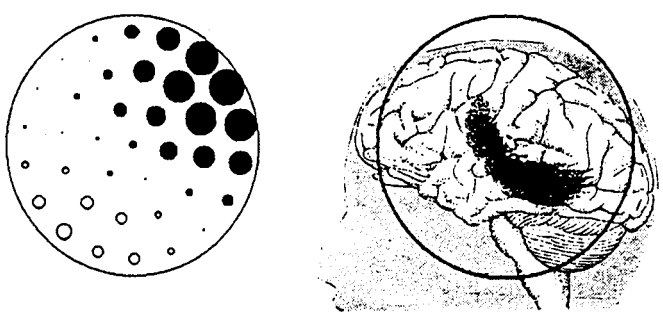

(a) (b)

Fig. 6. Neural activity at 110 ms after hearing "ha". (a) MEG. (b) Estimated current dipole spectrum distribution.

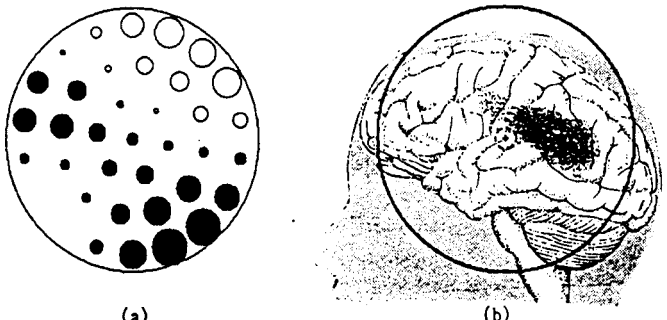

(a) (b)

Fig. 7. Neural activity at 160 ms after hearing "ha". (a) MEG. (b) Estimated current dipole spectrum distribution.

REFERENCES

[1] H. Carr, E. M. Purcell, *Phys. Rev.*, 94, p630, 1954.

[2] D. Cohen and D. McCaughan, "Magnetocardiograms and their variation over the chest in the normal subjects," *Am. J. Cardiol.*, 29, pp. 678-685, 1972.

[3] T. Katila, "Functional localization studies in magnetocardiography," *Int. J. Appl. Electromag. Matrls, Elsevier*, vol. 1, Nos. 2-4, pp. 179-187, Dec. 1990.

[4] A. Takeuchi, K. Watanabe, M. Nomura, S. Ishihara, M. Sumi, M. Murakami, K. Saito, Y. Nakaya and H. Mori, "The P wave in the magnetocardiogram," *J. Electrocardiol.*, 21 (2), pp. 161-167, 1988.

[5] S. J. Williamson and L. Kaufman, "Application of SQUID sensors to the investigation of neural activity in the human brain," *IEEE Trans. Magn.*, vol. MAG-19, no. 3, pp. 835-844, May 1983.

[6] S. Kuriki and F. Takeuchi, "Measurements of auditory evoked fields and analysis of their sources," *J. Japan Biomag. Bioelectromag. Soci.*, vol. 5, no. 1, pp. 20-23, Jun. 1992.

[7] Y. Saito, E. Itagaki and S. Hayano, "A formulation of the inverse problems in magnetostatic fields and its application to a source position searching of the human eye fields," *J. Appl. Phys.*, vol. 67, no. 9, pp. 5830-5832, May 1990.

[8] H. Saotome, K. Kitsuta, S. Hayano and Y. Saito, "Inverse problem in biomagnetic fields," *Trans. IEE Japan*, vol. 112-A, no. 4, pp. 279-286, Apr. 1992.

[9] H. Saotome, K. Kitsuta, S. Hayano and Y. Saito, "An estimation method of current distribution in biological systems by the sampled pattern matching method," *Trans. IEE Japan*, vol. 113-C, no. 1, pp. 69-76, Jan. 1993.

[10] H. Saotome, K. Kitsuta, S. Hayano and Y. Saito, "A neural behavior estimation by the generalized correlative analysis," *IEEE Trans. Magn.*, Mar. 1993.

[11] H. Saotome, K. Kitsuta, S. Hayano and Y. Saito, "Electromagnetic field source searching from the local field measurement," *Int. J. Appl. Electromag. Matrls, Elsevier*, 1993 (in press).

[12] H. Saotome, T. Doi, S. Hayano and Y. Saito, "Crack identification in metallic materials," *IEEE Trans. Magn.*, Mar. 1993

[13] J. C. Mosher, P. S. Lewis and R. M. Leahy, "Multiple dipole modeling and localization from spatio-temporal MEG data," *IEEE Trans. Biomed. Eng.* vol. BME-39, pp. 541-557, June 1992.

[14] J. Z. Wang, S. J. Williamson and L. Kaufman, "Magnetic source images determined by a lead-field analysis: The unique minimum-norm least-squares estimation," *IEEE Trans. Biomed. Eng.* vol. BME-39, pp. 665-675, June 1992.